A novel error mapping of bi-directional angular positioning deviation of rotary axes in a SCARA-type robot by "open-loop" tracking interferometer measurement

Soichi Ibaraki[a], Ryota Usui[a]

[a]*Department of Mechanical Systems Engineering, Hiroshima University*
Kagamiyama 1-4-1, Higashi Hiroshima, 739-8527, Japan. Phone/Fax: +81-82-424-7580

Type of contribution: Original research paper

Abstract

To further extend the application of an industrial robot to e.g. the machining, it is crucial to ensure its three-dimensional (3D) positioning accuracy over its entire workspace. Numerous past works presented numerical compensation based on the robot kinematic model containing position and orientation errors of rotary axes average lines, widely known as Denavit-Hartenberg (D-H) parameters. This paper presents two novel contributions. First, this paper proposes a kinematic model with the angular positioning deviation "error map" of each rotary axis, which is given as a function of command angular positions. Furthermore, to model the backlash influence, it is modeled dependent also on the direction of rotation. The second contribution is on the proposal of the "open-loop" tracking interferometer measurement to indirectly identify the angular positioning deviation of each rotary axis.

Email address: ibaraki@hiroshima-u.ac.jp (Soichi Ibaraki)

It measures the distance from the retroreflector, fixed on the table, to the robot's end effector at many points over the entire workspace by using a laser interferometer attached to the robot's end effector. The identified kinematic model's accuracy is experimentally investigated, and is compared to the conventional D-H model.
Keywords: SCARA robot, error calibration, volumetric accuracy, tracking interferometer, kinematic model

---

1. Introduction

In today's industry, industrial robots are mostly programmed by the teach method, where a human operates the robot manually by using a teach pendant, and the robot memorizes it. On the other hand, NC (numerically controlled) machine tools are typically programmed on a CAM (computer-aided manufacturing) software based on a 3D model of workpiece. This difference is partly due to a robot's significantly lower volumetric accuracy; a human operator's manual adjustment is often inevitable to successfully perform the given task. The *volumetric accuracy*, the term in [1], represents the 3D positioning accuracy over the entire workspace. If a robot is ensured to have higher volumetric accuracy, its application can be significantly expanded. One of its potential applications is the machining. The review paper [2, 3, 4] presented recent numerous works on robotic machining.

Lower stiffness is an inherent issue for industrial robots, particularly for machining applications. In many industrial robotic machining applications, a workpiece is chosen such that it does not give significant cutting forces. For example, when a workpiece is made by "near-net" casting [5], the depth of cut in its machining processes can be minimized. Typically, machining operations cannot be teach-programmed. When a robot is offline-programmed based on a virtual model, a robot is critically required to have sufficient volumetric accuracy over the entire working space. As the offline programming is expected to grow in various industrial robot applications, it becomes more important to ensure a robot having higher volumetric accuracy [6].

For a robot to have higher volumetric accuracy, numerous research efforts have been devoted to a model-based compensation. Its review can be

found in [6, 7, 8, 9]. Past works can be categorized, firstly, by the model used. Some works are based on the model containing link length errors and rotary axis angular offsets [10, 11, 12, 13]. More recent works employ the model with a full set of position and orientation errors of rotary axis average lines [14, 15, 16, 17, 18, 19]. The *axis average line*, the term defined in [1], represents the mean position and orientation of the axis of rotation. The position and orientation errors of rotary axis average lines are often called the D-H (Denavit-Hartenberg) parameters in the literature.

Even when these errors are compensated, in many cases a robot's volumetric error is still roughly 10 to 100 times larger than typical machine tools [13, 6]. Many works discussed the influence of joint compliance and friction [20, 21]. An interesting result was reported by Nubiola et al. [22]. They measured the angular positioning deviation of each rotary axis independently by using a laser tracker, which clearly showed nonlinear influence of link weights and friction. More researchers [23, 15, 24] recently presented the modeling of such an "residual" error, but they adopted a non-geometric model, such as a neural network model. A notably unique work was reported in 2018 by Hörler et al. [25]. They measured the angular positioning deviation of two rotary axes in a SCARA-type robot, and modelled it as a function of command angular position. The kinematic model presented in this paper adopts the same modeling scheme. While Hörler et al. [25] directly measures the end effector orientation by a special measuring instrument (a fiber positioner system for massive spectroscopic surveys), this paper adopts a laser interferometer widely used for error calibration of e.g. machine tools. Hörler et al. also measured the backlash (hysteresis) of each axis but its inclusion

into the kinematic model was not clearly presented in [25].

Past works can be categorized, secondly, by an instrument to measure the robot end effector's position. Many recent works use either a tracking interferometer (the term in [1], or a laser tracker) [13, 14, 15, 16, 20, 22] or a vision-based measurement system [10, 11, 17, 18, 19]. One practical issue is its higher cost. Another potential issue is their measurement uncertainty. It is significantly higher than measuring instruments used for machine tool error calibration, e.g. a laser interferometer.

This paper presents two original contributions. First, a novel kinematic model is proposed to significantly improve its prediction accuracy. The conventional D-H model, employed in many past works, is constructed based on the local coordinate systems aligned to the axis average lines. During the rotation of a rotary axis, its axis of rotation may displace or tilt. The axis average line represents its mean position and orientation only. This paper proposes a model including the angular positioning deviation of each rotary axis, which cannot be described by the position and orientation of the axis average lines. The *angular positioning deviation* represents the actual angular position of a rotary axis minus the command angular position in the plane perpendicular to the axis of rotation [1]. In a robot rotary axis, it is typically caused by the pitch error of a gear or a timing belt, or the joint compliance. Therefore, it cannot be constant – this paper models it as a function of the command angular position. Furthermore, a robot rotary axis can be subject to significant influence of gear backlash. To model it, the proposed model is dependent also on the direction of rotation.

This paper's second novel contribution is on the proposal of a scheme

to identify the angular positioning deviation profile of each rotary axis by measuring the distance to the robot's end effector. A laser interferometer is attached to a robot's end effector. When the robot's end effector is positioned at the given set of command positions, its orientation is regulated such that the laser beam is oriented to a retroreflector, fixed on the table.

The proposed scheme is called the "open-loop" tracking interferometer measurement in this paper. A conventional tracking interferometer automatically regulates the laser beam direction to follow the retroreflector by feedback control based on the reflected laser spot position. In the proposed scheme, the end effector's angular position is calculated based on its command position and the pre-estimated retroreflector position – in an "open-loop" control manner. Lower implementation cost is its major practical advantage. This scheme was proposed for machine tools by Ibaraki et al. [26, 27, 28, 29]. This paper's scheme can be seen as its extension to an industrial robot. While the algorithms in [26, 27, 28, 29] are for machine tools with three linear axes orthogonal to each other, this paper reformulates them for a robot kinematics.

Its measurement uncertainty can be potentially lower than a conventional tracking interferometer. For a conventional tracking interferometer, the uncertainty in the angle measurement of laser beam direction imposes significant contribution on the 3D position measurement uncertainty. The multilateration [1, 30, 31] is based only on the distances, and thus it generally has significantly lower measurement uncertainty. The application of the multilateration to machine tool error calibration has been long studied and now is commercially available [30]. This paper's scheme can be seen as its

extension to an industrial robot.

Fundamental ideas in this paper come from machine tool error calibration. For machine tools, the volumetric error compensation [32] is available on many latest CNCs (computerized numerical controllers), where error motions of each axis are modelled as a function of command position – as an "error map." Many schemes are available to indirectly identify the error maps from the tool center point position measurement (see a review in [33, 34]). Typical machine tools have orthogonal X, Y and Z axes. This paper reconstructs the multilateration-based error calibration scheme for robot kinematics.

This paper studies its application to the 2D positioning by a SCARA (Selective Compliance Assembly Robot Arm)-type robot (see Fig. 1). It has a simpler kinematics and significantly less error parameters than a 6 DOF (degrees of freedom) robot. It should be emphasized that a SCARA robot is usually not for the applications requiring higher rigidity. We do not intend to apply a SCARA robot to machining operations. The application to a SCARA robot is studied to investigate the fundamental validity and performance of this new methodology. Potential benefits with the improved volumetric accuracy of a SCARA robot include significant reduction of time and effort for the teaching of robot tasks, or possibly, its complete elimination (offline programming). The improved volumetric accuracy may further extend the robot's new applications, e.g. the geometric measurement by installing a touch-triggered probe or a non-contact scanner at end effector. The extension of the proposed scheme to a 6 DOF robot will be studied in our next research step.

2. Proposed measurement scheme

This paper targets a SCARA-type robot shown in Fig. 1. The 2D positioning accuracy by J_1- and J_2-axes on the XY plane is considered in this paper. The robot has J_3- and J_4-axes to translate/rotate the end effector to/around the Z-axis, but their accuracy is out of the algorithm's scope. The nominal link lengths are shown in Table 1 ("Nominal value").

Figure 1 illustrates the proposed measurement scheme. A laser interferometer is attached to the end effector such that its direction can be regulated by J_4-axis. The laser beam approximately intersects with the J_4-axis of rotation. The laser beam is approximately in the X-direction when $\theta_4 = 0°$, where θ_4 is the J_4 -axis angular position. A cat's eye retroreflector is fixed on the floor. A cat's eye retroreflector is a spherical glass of sufficiently high geometric accuracy with its hemispheric surface coated by the total-reflection metal-film deposition [35]. Its position is roughly estimated as $P_j = (P_{j,x}, P_{j,y}) \in \mathbb{R}^2$. When the k-th command position of the end effector is given by $p^*(k) = (p_x^*(k), p_y^*(k)) \in \mathbb{R}^2$ (the superscript "$*$" represents commanded values throughout this paper), the laser beam is directed to the retroreflector by regulating the J_4-axis angular position, $\theta_4^*(k)$, such that:

$$\tan\theta_4^*(k) = \frac{P_{j,y} - p_y^*(k)}{P_{j,x} - p_x^*(k)} \tag{1}$$

See Fig. 2. At each command position, the distance from the end effector to the retroreflector is measured. It is emphasized that the proposed scheme measures the distance only; the orientation of the laser beam is not used in the calculation in Section 3. This is repeated at different retroreflector positions, $j = 1, \cdots, N_t$.

Clearly, the estimation error of the retroreflector position, and the J_4-axis angular positioning error, can result in an error in the laser beam direction. Their influence will be discussed in Section 5.

Remark 1: The position of the retroreflector center can be roughly estimated as follows: position the end effector at $p^*_{\text{search}}(k) \in \mathbb{R}^2$. By manually rotating the J_4-axis, search for the J_4-angle, $\theta_4(k)$, such that the laser beam is directed to the retroreflector and comes back the interferometer. This is repeated at $k = 1, \cdots, N_{\text{search}}$. The command end effector positions, $p^*_{\text{search}}(k)$, should be selected such that they cover the entire workspace.

When $\theta_4 = 0$, the laser beam is aligned approximately to the X-axis direction but it can have significant alignment error. This orientation is represented by $\theta_{40} \in \mathbb{R}$. From the searched set of $\theta_4(k)$ $(k = 1, \cdots, N_{\text{search}})$, the retroreflector position, $P_j = (P_{j,x}, P_{j,y})$, and the J_4-axis angular offset, θ_{40}, can be identified by solving the following minimization problem:

$$\min_{P_{j,x}, P_{j,y}, \theta_{40}} \sum_{k=1,\cdots,N_{\text{search}}} \left\{ \theta_4(k) - \left(\tan^{-1} \left(\frac{P_{j,x} - p^*_{\text{search},x}(k)}{P_{j,y} - p^*_{\text{search},y}(k)} \right) - \theta_{40} \right) \right\}^2 \tag{2}$$

Remark 2: The laser interferometer's horizontal position should be adjusted such that the laser beam approximately intersects with the J_4-axis of rotation. This can be done as follows: orientate the laser beam to a retroreflector. Rotate J_4-axis within the range where the laser displacement is measurable. Adjust the interferometer's position such that the variation in the measured displacement is minimized.

Remark 3: The influence of the misalignment of the laser beam position from the J_4-axis of rotation on the measurement uncertainty will be discussed

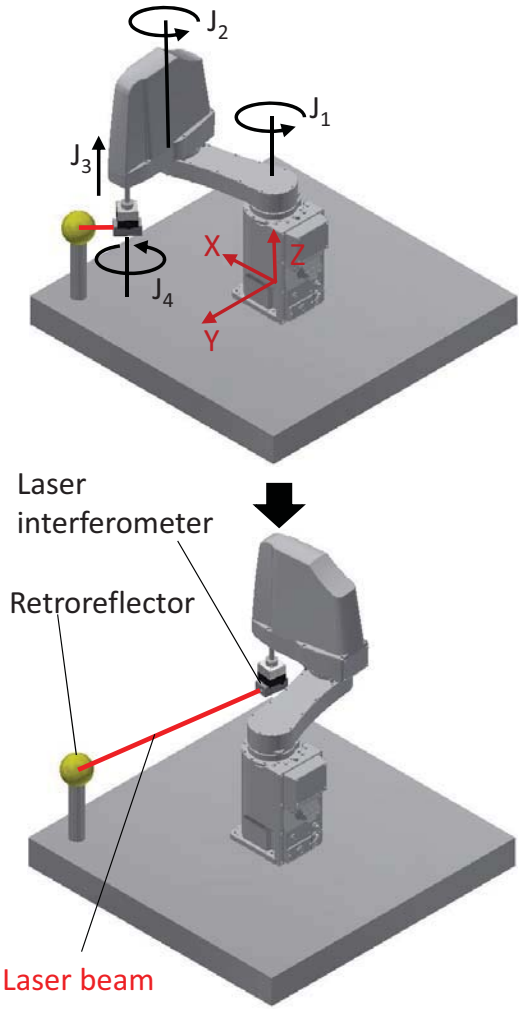

Figure 1: The SCARA robot configuration and the proposed "open-loop" tracking measurement scheme.

in Section 5.

Table 1: Link lengths and joint angular offset. $*$: In the proposed model, the angular offset is included in the J_2-axis angular positioning deviation shown in Fig. 6b.

Error parameter	Nominal value	Identified (Conventional)	Identified (Proposed)
Link 1 length, L_1	325.0 mm	324.971 mm	324.964 mm
Link 2 length, L_2	225.0 mm	225.004 mm	224.998 mm
J_2-axis angular offset, θ_{20}	0	-5.55 mdeg	$*$

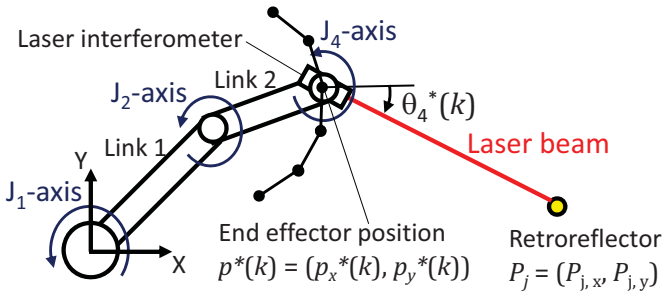

Figure 2: Measurement setup.

3. Identification of bi-directional angular positioning deviation of rotary axes

3.1. Conventional error calibration algorithm

As reviewed in Section 1, most of the past works [9-16] employ the kinematic model containing the D-H parameters only. During the rotation of a rotary axis, its axis of rotation may displace or tilt. The line representing its mean position and orientation is called *the axis average line* in [1]. The conventional D-H model is constructed based on the local coordinate sys-

tems aligned to the axis average lines. The D-H parameters represent the position and orientation of one local coordinate system respect to the other. For the 2D positioning by a SCARA-type robot, when the end effector Z-displacement and orientation errors are not considered, the following three parameters, shown in Table 1, are the D-H parameters: the length of Link 1, L_1, the length of Link 2, L_2, and the J_2-axis angular offset, θ_{20}. As a basis for the proposed algorithm presented in Section 3.2, this subsection first presents an algorithm to identify them. The measurement scheme in Section 2 is new but the algorithm presented here can be seen conventional.

When command J_1- and J_2-axis angular positions are respectively given by $\theta_1^*(k)$ and $\theta_2^*(k)$ $(k = 1, \cdots, N)$, the end effector's position in the XY plane is given by the following kinematic model with the three parameters in Table 1. The origin of the coordinate system is at the J_1-axis of rotation (see Fig. 2).

$$\hat{p}(k) = \begin{bmatrix} L_1 \cos(\theta_1^*(k)) + L_2 \cos(\theta_1^*(k) + \theta_2^*(k) + \theta_{20}) \\ L_1 \sin(\theta_1(k)) + L_2 \sin(\theta_1^*(k) + \theta_2^*(k) + \theta_{20}) \end{bmatrix} \tag{3}$$

In the measurement scheme in Section 2, the retroreflector positions, P_j, can be estimated only roughly. Furthermore, a laser interferometer can only measure the displacement relative to the laser beam initial length. This initial length, i.e. $d_{0j} \equiv \|\hat{p}(1) - P_j\|$, is called the dead path length. The present algorithm identifies them too. Define the parameters to be identified by:

$$e_{\text{conventional}} = \left[L_1, L_2, \theta_{20}, P_1^T, \cdots, P_{N_t}^T, d_{01}, \cdots, d_{0N_t}\right] \in \mathbb{R}^{3+3N_t} \tag{4}$$

Suppose that the measured laser displacement between the k-th command end effector position, $p^*(k)$, and the retroreflector position, P_j, is given by

$d_j(k) \in \mathbb{R}$. Then, $e_{\text{conventional}}$ in Eq. (4) can be estimated by solving the following problem:

$$\min_{e_{\text{conventional}}} \sum_{k=1,\cdots,N, j=1,\cdots,N_t} \left(\|\hat{p}(k) - P_j\| - d_{0j} - d_j(k)\right)^2 \tag{5}$$

3.2. Proposed algorithm

3.2.1. The proposed kinematic model and error parameters to be identified

Some past works, e.g. [22, 23, 15, 24], or the experiment in Section 4.3 (Fig. 11c), showed that the kinematic model (3), with the error parameters in Table 1, cannot model the robot's 2D positioning error in a sufficient accuracy. This paper proposes to model this "residual" error by including the angular positioning deviation of J_1- and J_2-axes into the kinematic model. The angular positioning deviation of a rotary axis is typically caused by the transmission (a timing belt or a gear) pitch error or the joint compliance, and thus is a function of its command angular position. Furthermore, robot joints are generally subject to significant backlash. To take its influence into consideration, the angular positioning deviation of each rotary axis is modeled dependent also on the rotation direction.

Denote the i_n-th nominal (command) angular position of the J_n-axis ($n = 1, 2$) by $\theta^*_{n,\text{map}}(i_n) \in \mathbb{R}$ ($i_n = 1, \cdots, N_n$). The angular positioning deviation of the J_n-axis at this angle is represented by $\Delta\theta_{n,\text{map}}(i_n, \text{sgn}(\dot{\theta}^*_n(i_n)))$, where $\text{sgn}(\dot{\theta}^*_{n,\text{map}}(i_n))$ is +1 (or -1) when $\dot{\theta}^*_{n,\text{map}}(i_n) \geq 0$ (or $\dot{\theta}^*_{n,\text{map}}(i_n) < 0$). $\dot{\theta}^*_{n,\text{map}}(i_n)$ represents the angular velocity of J_n-axis at $\theta^*_{n,\text{map}}(i_n)$.

The objective of the present algorithm is to identify:

$$\begin{aligned} e &= \big[L_1, L_2, P_1^T, \cdots, P_{N_t}^T, d_{01}, \cdots, d_{0N_t}, \\ &\quad \Delta\theta_{1,\mathrm{map}}(1,+1), \cdots, \Delta\theta_{1,\mathrm{map}}(N_1,+1), \\ &\quad \Delta\theta_{1,\mathrm{map}}(1,-1), \cdots, \Delta\theta_{1,\mathrm{map}}(N_1,-1), \\ &\quad \Delta\theta_{2,\mathrm{map}}(1,+1), \cdots, \Delta\theta_{2,\mathrm{map}}(N_2,+1), \\ &\quad \Delta\theta_{2,\mathrm{map}}(1,-1), \cdots, \Delta\theta_{2,\mathrm{map}}(N_2,-1)] \\ &\quad \in \mathbb{R}^{2+3N_t+2N_1+2N_2} \end{aligned} \tag{6}$$

Such representation of the angular positioning deviation is called the "error map" in this paper.

3.2.2. Identification Algorithm

In the measurement scheme in Section 2, suppose that the command J_n-axis angular position ($n = 1, 2$) is given by $\theta_n^*(k)$. The angular positioning error at this angle is parameterized by a linear interpolation of $\theta_{n,\mathrm{map}}^*(i_n, \pm 1)$ as follows:

$$\begin{aligned} \theta_1(k) &= \theta_1^*(k) + \alpha_1(k) \cdot \Delta\theta_{1,\mathrm{map}}(i_1, \mathrm{sgn}(\dot{\theta}_1(k))) \\ &\quad + (1 - \alpha_1(k)) \cdot \Delta\theta_{1,\mathrm{map}}(i_1 + 1, \mathrm{sgn}(\dot{\theta}_1(k))) \\ \theta_2(k) &= \theta_2^*(k) + \alpha_2(k) \cdot \Delta\theta_{2,\mathrm{map}}(i_2, \mathrm{sgn}(\dot{\theta}_2(k))) \\ &\quad + (1 - \alpha_2(k)) \cdot \Delta\theta_{2,\mathrm{map}}(i_2 + 1, \mathrm{sgn}(\dot{\theta}_2(k))) \end{aligned} \tag{7}$$

where i_n ($n = 1, 2$) meets:

$$\theta_{n,\mathrm{map}}^*(i_n) \leq \theta_n^*(k) \leq \theta_{n,\mathrm{map}}^*(i_n + 1) \tag{8}$$

The interpolation weights, $\alpha_n(k)$ ($n = 1, 2$) , are given by:

$$\alpha_n(k) = \frac{\theta_n^*(k) - \theta_{n,\mathrm{map}}^*(i_n)}{\theta_{n,\mathrm{map}}^*(i_n + 1) - \theta_{n,\mathrm{map}}^*(i_n)} \tag{9}$$

When J_1- and J_2-axes are respectively commanded at $\theta_1^*(k)$ and $\theta_2^*(k)$, the actual end effector position, $\hat{p}(k)$, is formulated by substituting $\theta_1(k)$ and $\theta_2(k)$ in Eq. (7) into $\theta_1^*(k)$ and $\theta_2^*(k)$ in Eq. (3). When the measured laser displacement between the command end effector position, $p^*(k)$, and the retroreflector position, P_j, is given by $d_j(k)$, the error parameters, e in Eq. (6), can be estimated by solving the following minimization problem:

$$\min_{e} \sum_{k=1,\cdots,N, j=1,\cdots,N_t} \{\|\hat{p}(k) - P_j\| - d_{0j} - d_j(k)\}^2 \tag{10}$$

An iterative linearization-based approach can be used to locally solve the problem (10).

Remark 1: When the number of the retroreflector positions, N_t, is three or more, the end effector's actual 2D position, $p(k)$, can be calculated by applying the multilateration algorithm presented in [31] ($N_t = 2$ is sufficient only if the retroreflector positions are exactly known). This implies that the problem (10) is generally solvable when $N_t \geq 3$. When $N_t < 3$, and the number of the unknowns, i.e. $2 + 3N_t + 2N_1 + 2N_2$ in Eq. (6), is larger than the number of the measurements, i.e. $N \cdot N_t$ in Eq. (10), then the problem (10) may be solvable but the uncertainty can be significantly higher.

Remark 2: It is well known that the uncertainty in the multilateration measurement can strongly depend on the setup of the fixed stations (retroreflector positions in this paper's case) [30, 31]. For example, in the setup shown in Fig. 5, three reflector positions, P_1 to P_3, lay almost in a line. It is predictable that the uncertainty would be significantly larger if the end effector is on this line. The uncertainty analysis, presented in Section 5, is essential for the design of retroreflector positions.

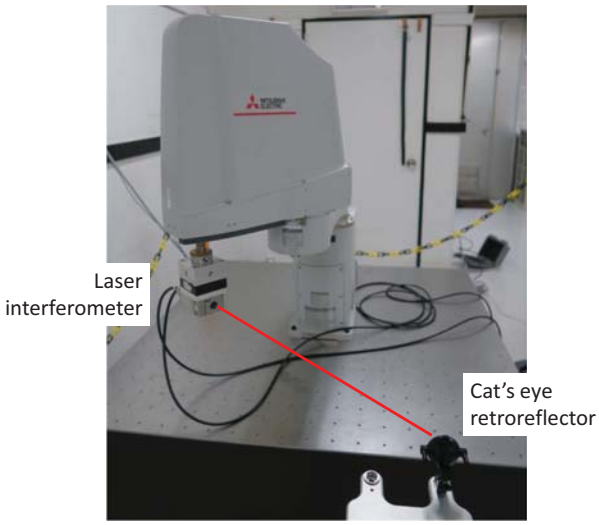

Figure 3: Experimental setup.

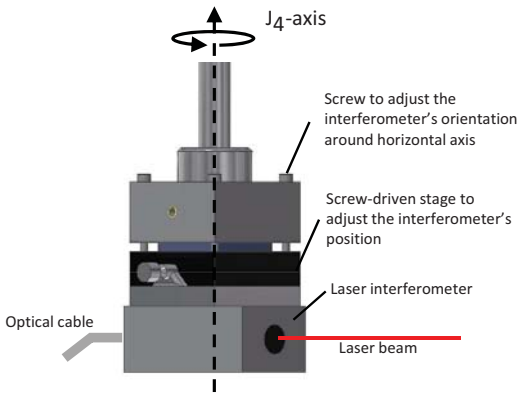

Figure 4: Installation setup of the laser interferometer at the robot's end effector.

4. Experiment

4.1. Experimental setup

A SCARA-type robot, RH-3FRH-5515-D by Mitsubishi Electric Corp. was used. Figure 3 shows the experimental setup. The angular positioning

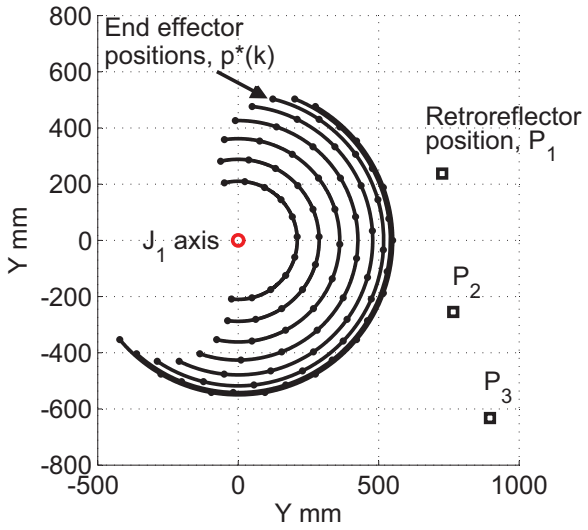

Figure 5: End effector command positions, $p^*(k)$, and retroreflector positions, P_1, P_2 and P_3.

resolution of J_1-, J_2-, and J_4-axes is 1 mdeg. Their encoder resolution is not disclosed by the manufacturer. The positioning repeatability is, according to the manufacturer's specifications, ± 0.012 mm in X-Y composite, and $\pm 0.004°$ for J_4-axis. The laser interferometer, Distax L-IM-300A by Tokyo Seimitsu Co., Ltd., was used. It was attached to the robot's end effector via a screw-driven stage as shown in Fig. 4. The interferometer's horizontal position can by adjusted by it such that the laser beam approximately intersects with the J_4-axis of rotation. Furthermore, its orientation can be adjusted by vertical screws such that the laser beam is approximately parallel to the robot's XY plane. The cat's eye retroreflector by Etalon AG was used (viewing angle: $\pm 80°$, optical form deviation (circularity): $< 0.2\mu$m).

Figure 5 shows the end effector command positions, $p^*(k)$ $(k = 1, \cdots, 176)$.

The J_2-axis is indexed at:

$$\theta_2^* = [0^\circ, 20^\circ, \cdots, 140^\circ, 140^\circ, 120^\circ, \cdots, 0^\circ] \in \mathbb{R}^{16} \tag{11}$$

This is repeated at each of the J_1-axis angular positions:

$$\theta_1^* = [-140^\circ, -120^\circ, \cdots, 60^\circ, 60^\circ, 40^\circ, \cdots, -140^\circ] \in \mathbb{R}^{22} \tag{12}$$

Note that all the command points are positioned bidirectionally. The number of command positions is thus $N = 22 \times 16 = 352$. In Fig. 5, three retroreflector positions, P_j ($j = 1, 2, 3$, $N_t = 3$), are also shown. The same measurement was repeated for each retroreflector position.

4.2. Error identification

First, the conventional algorithm, presented in Section 3.1, was applied to identify link lengths, L_1 and L_2, and the J_2 angular offset, θ_{20}. Table 1 ("Identified (Conventional)") shows the identified values. Then, by applying the algorithm proposed in Section 3.2, the bidirectional angular positioning deviations of J_1- and J_2-axes, a) $\Delta\theta_{1,\mathrm{map}}(i_1, \pm 1)$ and b) $\Delta\theta_{2,\mathrm{map}}(i_2, \pm 1)$, are identified as shown in Fig. 6. The difference in the identified deviations in positive and negative directions shows the backlash influence. Table 1 ("Identified (Proposed)") shows L_2, J_2 and θ_{20} identified by the proposed algorithm.

Remark 1: in a machine tool, the bi-directional angular positioning deviation of a rotary axis is typically measured by using e.g. a laser autocollimator and a reference indexing table or an optical polygon [36]. Such a direct measurement is difficult or impossible for a robot, since it is generally difficult

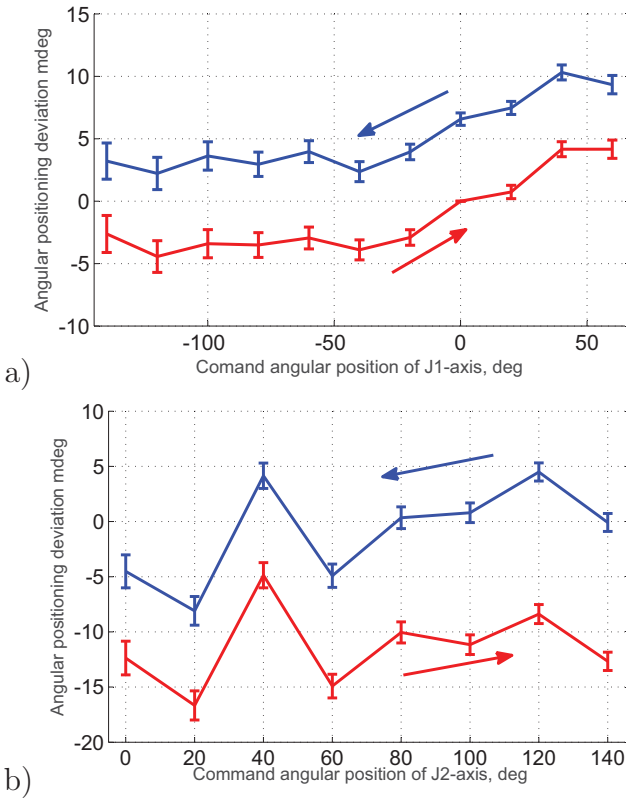

Figure 6: Identified bi-directional angular positioning deviations, $\Delta\theta_{n,\mathrm{map}}(i_n, \pm 1)$ for a) J_1-axis ($n = 1$), b) J_2-axis ($n = 2$). Red: for positive direction ($+1$) and blue: for negative direction (-1). Error bars represent the uncertainty ($k = 1$) in the estimates (see Section 4)

to install a reference mirror on the axis of rotation. The proposed scheme indirectly estimates it by measuring the distance to the robot's end effector at many points.

Remark 2: This robot's J_1 and J_2 axes are driven via a speed reducer and its backlash is often caused by the elastic deformation of the gear or other components. Approximately constant difference in bidirectional angular po-

sitioning deviation profiles is likely caused by such elastic deformation.

4.3. Experimental validation

The prediction accuracy of the proposed model was compared to the conventional model with the D-H parameters only. On the path shown in Fig. 7 ("Measured path") ($X = 200$ mm and $Y = -500$ to 500 mm), the robot's 2D positioning error was measured by using a commercial tracking interferometer, AT960-XR by Leica Geosystem (the measurement uncertainty: $U_{xyz} = \pm 15\mu\text{m} + 6\mu\text{m/m}$, according to the manufacturer's specifications) . Figure 8 shows the measurement setup.

Figure 9 compares the measured trajectory in the Y-direction, i.e. the bidirectional linear positioning deviation in Y direction, E_{YY}, with a) its estimates by the conventional D-H model and b) the estimates by the proposed model. The conventional D-H model is given by Eq. (3) with the three D-H parameters, i.e. the link lengths, L_1 and L_2, and the J_2 angular offset, θ_{20}. The proposed model is given by Eq. (3) with the identified J_1- and J_2-axis angular positioning deviations shown in Fig. 6, in addition to the D-H parameters. Similarly, Fig. 10 compares the measured trajectory in the X-direction, i.e. the straightness deviation, E_{XY}, with a) its estimates by the conventional D-H model and b) the estimates by the proposed model.

Both Figs. 9a and 10a clearly show that the conventional D-H model has a significant prediction error from the measured trajectory. On the other hand, in Figs. 9b and 10b, the estimated deviations show a good match with the measured deviations.

For the comparison over the entire workspace, the 2D trajectory were measured by the tracking interferometer for the command trajectory shown

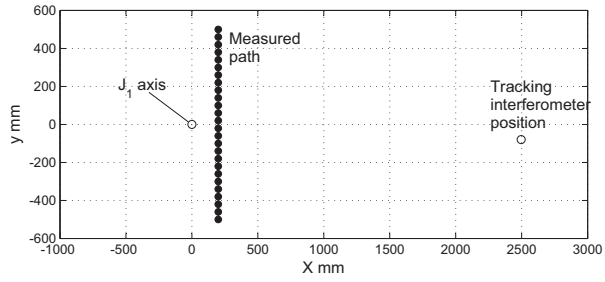

Figure 7: End effector path measured by the tracking interferometer.

Figure 8: Tracking interferometer measurement setup.

by black dots (•) in Fig. 11 (a to d). Figure 11a shows the measured trajectories (red and blue dots, ∘ and ○, for different directions). An error vector from command to measured positions is magnified 1,000 times, i.e. an error 200 μm is plotted as a vector of the length 200 mm (see "Error scale"). Figure 11b shows the estimated trajectory by the proposed model with the identified J_1- and J_2-axis angular positioning deviations. For the comparison, Fig. 11c shows the trajectory estimated by the conventional D-H model.

When compared to the measured trajectory in Fig. 11a, the conventional

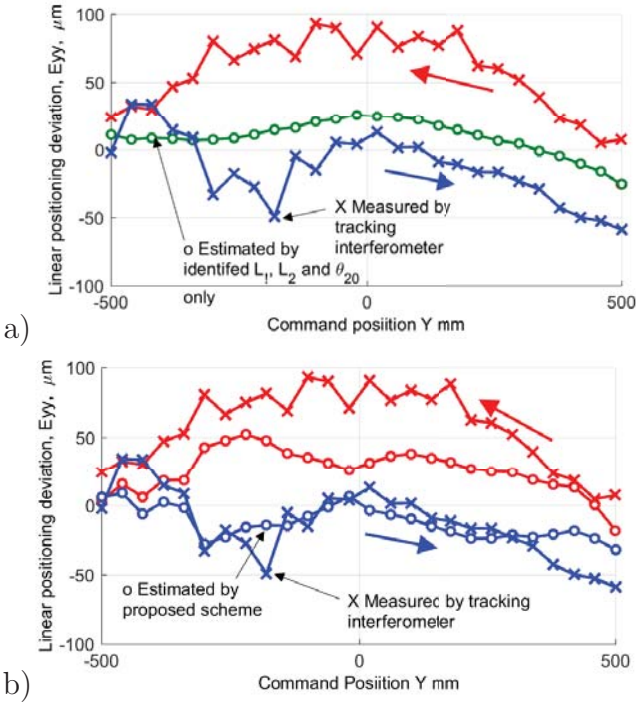

Figure 9: Comparison in the bidirectional linear positioning deviation in Y direction, E_{YY}, between the measured trajectory by the tracking interferometer (x in red and blue for different directions) and a) its estimates by the conventional D-H model (∘ in green) and b) it estimates by the proposed model (∘ in blue and red for different directions).

model (Fig. 11c) clearly cannot predict the 2D positioning accuracy in a sufficient accuracy. On the other hand, the proposed model (Fig. 11b) shows significantly higher prediction accuracy. It is emphasized that the tested path (black dots (•)) is completely different from the path used in the error calibration (Fig. 5). Figure 11d shows the difference of the trajectories measured by the tracking interferometer (Fig. 11a) and those estimated by the proposed model (Fig. 11b). If the robot's positioning repeatability is sufficiently high, Fig. 11d represents the positioning error when the identified

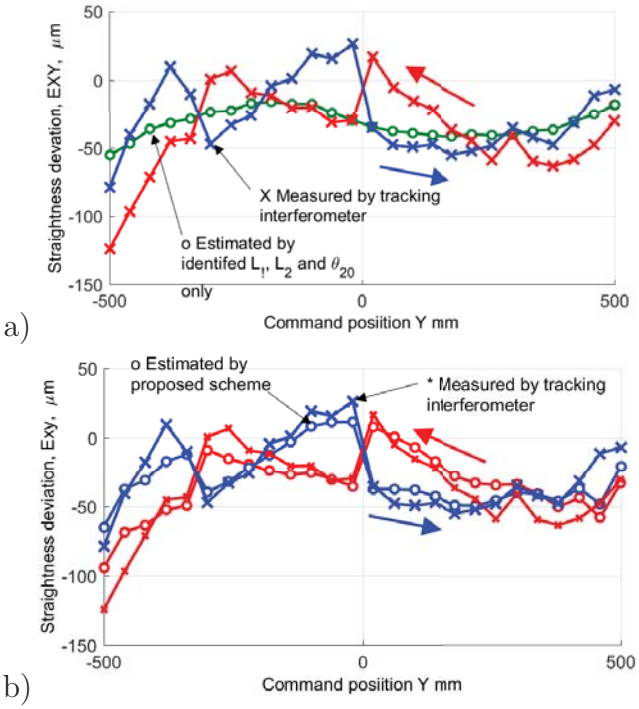

Figure 10: Comparison in the bidirectional straightness deviation in X for Y-motion, E_{XY}, at X=200 mm between the measured trajectory by the tracking interferometer (x in red and blue for different directions) and a) its estimates by the conventional D-H model (∘ in green) and b) its estimates by the proposed model (∘ in blue and red for different directions).

angular positioning deviations are compensated for.

Remark: In Fig. 11d, relatively larger estimation error can be observed in the mean Y-position at Path X1 (at Y380 mm). This may be partly attributable to the robot's thermal deformation caused by the temperature difference between the tracking interferometer measurement and the proposed measurement. Recent studies, e.g. [37], clarified that thermal influence on a robot's volumetric accuracy can be significant. Further investigation will be

left for our future research.

5. Uncertainty analysis

The proposed "open-loop" tracking measurement has uncertainty contributors that are in principle negligible in conventional automated tracking interferometers. The present uncertainty analysis emphasizes the investigation of their contribution.

Table 2 shows the extended uncertainty, $U(k = 1)$ (k: coverage factor), of the laser displacement when the end effector is located at $p^*(k) = (100, 100)$ mm and the retroreflector is at P_1 in Fig. 5. Some uncertainty contributions were assessed by actually measuring the experimental instrument, e.g. u_{21} to u_{23}. Others were assessed based on the instrument's catalogue. The uncertainty in the laser displacement depends on the position of the end effector and the retroreflector. Table 2 merely shows an example for a single point to illustrate each contributor's influence.

In the proposed "open-loop" tracking measurement, the laser beam direction is commanded by Eq. (1) based on the initial estimate of the retroreflector position, P_j, and the command end effector position, $p^*(k)$. Both can have a significant error. Furthermore, J_4-axis may have significant angular positioning error. They all cause an error in the laser beam direction. For the cat's eye retroreflector used in the experiment, the laser beam may deviate from its center by about 1 mm at maximum – if it is larger than this, the laser beam would not be reflected back to the interferometer. The uncertainty in the laser beam direction is assessed by this "maximum" deviation. Even with this large direction error, its contribution to the laser displacement

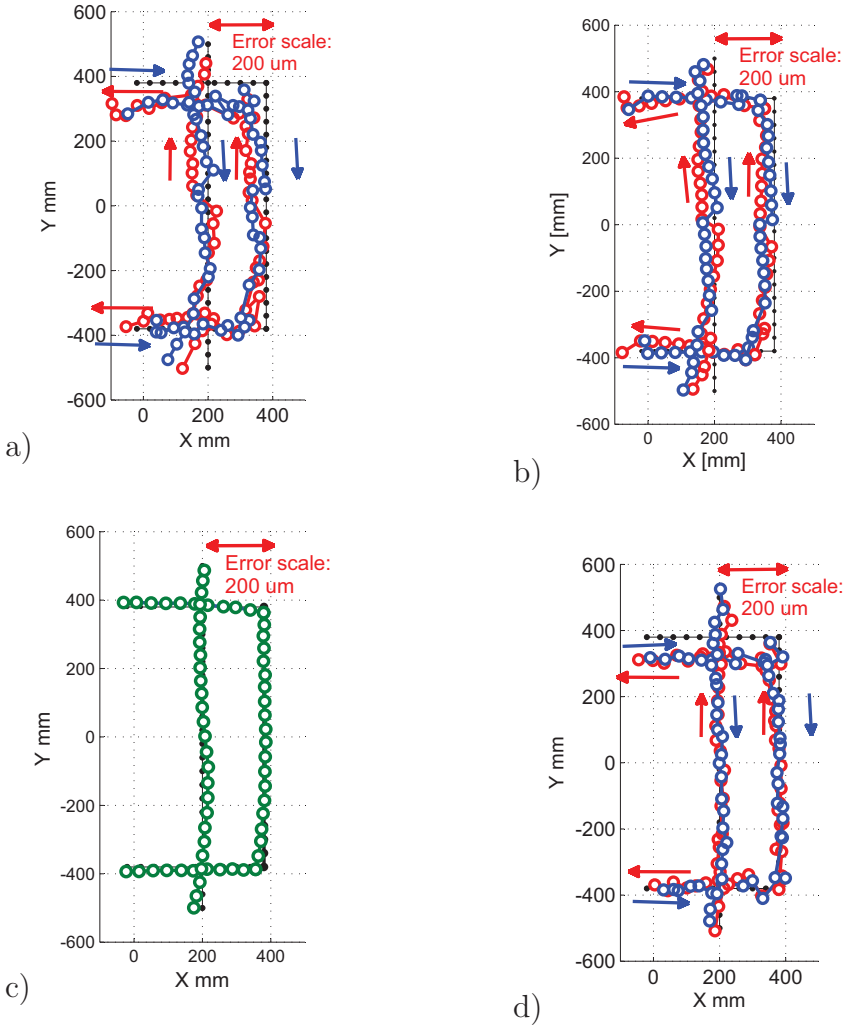

Figure 11: a) The 2D trajectory measured by the tracking interferometer, b) the one estimated by the proposed model with the identified J_1- and J_2-axis angular positioning deviations, c) the one estimated by the conventional D-H model, and d) the difference between a) and b). Red and blue dots (∘ and ∘) are for different directions (shown by red and blue arrows). Black dots (•) represent command positions. The positioning error from the command position is magnified 1,000 times ("Error scale").

Table 2: Uncertainty budget ($k = 1$) for laser displacement when the end effector is located at $p^*(k) = (100, 100)$ and the retroreflector is at P_1 in Fig. 5.

Symbol	Contributor		Uncertainty in laser displacement ($k = 1$)
u_1	Uncertainty in laser length		10 μm
	u_{11}	Wavelength accuracy	0.04 μm
	u_{12}	Wavelength correction	0.19 μm
	u_{13}	Environmental change	0.09 μm
	u_{14}	Robot's repeatability	10 μm
u_2	Uncertainty in interferometer position in laser direction		12 μm
	u_{21}	Radial error motion of J_1-axis	5 μm
	u_{22}	Radial error motion of J_2-axis	5 μm
	u_{23}	Radial error motion of J_4-axis	10 μm
u_3	Uncertainty due to laser beam orientation error		0.31 μm
	u_{31}	Uncertainty in laser beam orientation by J_1-axis	7.17×10^{-4} rad
	u_{32}	Uncertainty in laser beam orientation by J_2-axis	7.17×10^{-4} rad

is sufficiently small (u_{31} and u_{32} in Table 2), since it gives only the "cosine error."

There can be a significant misalignment error of the laser beam from the centerline of J_4-axis (see Remark 2 in Section 2). The laser beam is, however, nominally oriented to the retroreflector. If there is no orientation error, the influence of the laser beam misalignment error on the laser beam length is constant, regardless of the J_4-axis angle, and thus does not influence the test result at all. Since there exists the laser beam orientation error, its influence

is not zero, but it is negligibly small. The misalignment of the laser beam direction to the robot's XY plane only gives the "cosine error" on the measured displacement and thus negligibly small.

The uncertainty in the laser displacement at each command position propagates into the uncertainty in the estimated angular positioning deviations of J_1- and J_2-axes. This relationship can be described by Eqs. (3)(7) and (10), but is too complex to algebraically calculate the uncertainty propagation. In such a case, the Monte Carlo simulation can be applied for the uncertainty evaluation [38]. Analogous analysis is presented in [39, 27, 28]. The simulation procedure is outlined as follows: a measurement error of the laser displacment, $d_j(k)$, is given for every j and k as a normally distributed random number based on the uncertainty budget shown in Table 2. Then, solve the problem (10) to calculate e in Eq. (6). The standard deviation of each estimate is evaluated.

The contribution of the contributors in Table 2 on the uncertainty ($k = 1$) in the estimated angular positioning deviations is evaluated and shown by error bars in Fig. 6.

Remark: The present uncertainty evaluation based on Monte Carlo simulation is time-consuming. Olarra et al. [40] presented the uncertainty evaluation methodology based on the Jacobian matrix for the problem (10) with an application to parameter identification for a parallel kinematic robotic machine tool.

6. Conclusion and future work

The contributions of this study are summarized below.

- The conventional kinematic model of a robot only contains position and orientation errors of rotary axes average lines, widely known as the D-H parameters. The first major novel contribution of this paper is on the proposal of a kinematic model of a SCARA-type robot with the bidirectional angular positioning deviation "error map" of each rotary axis. The angular positioning deviation of a rotary axis is typically caused by the transmission pitch error or the joint compliance, and thus is a function of its command angular position. Furthermore, to model the influence of the gear backlash, it is modelled dependent also on the rotation direction. For the paths that are not included in the paths used for the model identification, the proposed model showed a significantly better prediction performance of the end effector's 2D positions compared to the conventional D-H model.

- The "open-loop" tracking interferometer test was proposed to indirectly identify the angular positioning deviation profile of the two rotary axes. For machine tools, the researchers [30, 31] developed the multilateration scheme to indirectly identify all the error motions of each linear axis. This paper's scheme can be seen as a novel extension to an industrial robot.

This paper only considered a SCARA-type robot. It is to investigate the effectiveness of the proposed model in the simplest robot kinematics, minimizing the influence of other potential error sources in a six-axis robot, such as the gravity influence that changes with a robot's pose. The first contribution of this paper, a kinematic model with the bidirectional angular positioning

deviation of each rotary axis, can be straightforwardly extended to the 3D positioning by a six-axis robot. The author's group started studying this extension (its preliminary result is presented in [41]). This paper presents the fundamental principle of the proposed model in a simplified robot kinematics.

This paper's second contribution, the "open-loop" tracking interferometer test, can be also potentially extended to a six-axis robot. Unlike the SCARA robot case, however, the regulation of laser beam direction will be three dimensional, which can makes it significantly more difficult or time-consuming to set up the initial laser beam direction and retroreflector position (see Remark in Section 2). Furthermore, more importantly, when this test is performed by a six-axis robot, all the six axes must be driven to direct the laser beam to a retroreflector. Unlike the SCARA robot case, it will not be possible to separately measure each rotary axis by this test. The extension of the proposed "open-loop" tracking measurement scheme to a six-axis robot is possible, but more careful study will be needed especially on the uncertainty in the estimation of the angular positioning deviation. This is left to our future research.

In this paper, the angular positioning deviation of each rotary axis is assumed dependent only on its command angle and rotation direction. Mainly due to the gravity influence, the position and orientation of the axis average line of a rotary axis, or its angular positioning deviation, can vary depending on the angular position of other axes. It is predictable that such an "axis-to-axis crosstalk" is more significant on a six-axis robot. Such an influence will be studied in our future research.

Acknowledgement

This work was supported in part by JSPS KAKENHI Grant Number JP18K03874.

References

[1] ISO 230-1:2012, Test code for machine tools – Part 1: Geometric accuracy of machines operating under no-load or quasi-static conditions.

[2] Uriarte L, Zatarain M, Axinte D, Yagüe-Fabra J, Ihlenfeldt S, Eguia J, Olarra A. Machine tools for large parts, CIRP Annals – Manufacturing Technology; 2013; 62 (2); 731-750.

[3] Verl A, Valente A, Melkote S, Brecher C, Ozturk E, Tunc LT, Robots in ma-chining, CIRP Annals – Manufacturing Technology; 2019; 68(2); 799-822.

[4] Chen Y, Dong F. Robot machining: recent development and future research issues. Int. J. Advanced Manufacturing Technology 2013; 66 (9); 1489-1497.

[5] Marini D, Cunningham D, Corney JR, Near net shape manufacturing of metal: A review of approaches and their evolutions, Proceedings of the Institution of Mechanical Engineers, Part B: Journal of Engineering Manufacture; 2018;232(4); 650-669.

[6] Ibaraki S, Theissen NA, Archenti A, Alam MM, Evaluation of Kinematic and Compliance Calibration of Serial Articulated Industrial Manipu-

lators, International Journal of Automation Technology; 2021; 15(5); 567-580.

[7] Van Brussel H. Evaluation and Testing of Robots, CIRP Annals; 1990; 39(2); 657-664.

[8] Hollerbach JM, Wampler CW. The calibration index and taxonomy for robot kinematic calibration methods, Int. J. Robotics Research; 1996; 15 (6) 573-591.

[9] Gang C, Tong L, Ming C, Xuan J, Xu S. Review on kinematics calibration technology of serial robots, Int. J. Precision Engineering and Manufacturing; 2014; 15(8); 1759-1774.

[10] Toyama S, Hatae S, Haga S, Kinoshita N, Kinematic Calibration of SCARA Robot with Condition Number and Error Map Method, CIRP Annals; 1991; 40(1); 9-12.

[11] Watanabe A, Sakakibara S, Ban K, Yamada M, Shen G. A Kinematic Calibration Method for Industrial Robots Using Autonomous Visual Measurement, Annals of CIRP; 2006; 55(1); 1-6.

[12] Messay T, Ordonez R, Marcil E. Computationally efficient and robust kinematic calibration methodologies and their application to industrial robots, Robotics and Computer-Integrated Manufacturing; 2016; 37; 33-48.

[13] Wu Y, Klimchik A, Caro S, Furet B, Pashkevich A. Geometric calibration of industrial robots using enhanced partial pose measurements and

design of experiments, Robotics and Computer-Integrated Manufacturing; 2015; 35; 151-168.

[14] Alici G, Shirinzadeh B: A systematic technique to estimate positioning errors for robot accuracy improvement using laser interferometry based sensing, Mechanism and Machine Theory; 2005; 40(8); 879-906.

[15] Gong C, Yuan J, Ni J. Nongeometric error identification and compensation for robotic system by inverse calibration, Int. J Machine Tools and Manufacture; 2000; 40(14); 2119-2137.

[16] Kohama A, Mori R, Komai S, Suzuki M, Aoyagi S, Fujioka J, Kamiya Y. Calibration of kinematic parameters of a robot using neural networks by a laser tracking system, Proc. of 7th Int. Conf. on Machine Automation; 2008; 251-256.

[17] Filion A, Joubair A, Tahan AS, Boneva IA. Robot calibration using a portable photogrammetry system, Robotics and Computer-Integrated Manufacturing; 2018; 49; 77-87.

[18] Meng Y, Zhuang H, Autonomous Robot Calibration Using Vision Technology, Robotics and Computer-Integrated Manufacturing; 2007; 23 (4); 436-446.

[19] Zhang X, Song Y, Yang Y, Pan H. Stereo vision based autonomous robot calibration, Robotics and Autonomous Systems; 2017; 93; 43-51.

[20] Slamani M, Nubiola A, Bonev IA. Modeling and assessment of the backlash error of an industrial robot, Robotica; 2012; 30 (7) 1167-1175.

[21] Ruderman M, Hoffmann F, Bertram T. Modeling and identification of elastic robot joints with hysteresis and backlash, IEEE Trans. on Industrial Electronics; , 56 (10) (2009) 3840-3847.

[22] Nubiola A, Bonev IA, Absolute calibration of an ABB IRB 1600 robot using a laser tracker, Robotics and Computer-Integrated Manufacturing; 2013; 29 (1); 236-245.

[23] Zhao G, Zhang P, Ma G, Xiao W. System identification of the nonlinear residual errors of an industrial robot using massive measurements, Robotics and Computer Integrated Manufacturing; 2019; 59; 104-114.

[24] Nguyen HN, Zhou J, Kang HJ, A calibration method for enhancing robot accuracy through integration of an extended Kalman filter algorithm and an artificial neural network, Neurocomputing; 2015; 151; 996-1005.

[25] Hörler P, Kronig L, Kneib JP, Bouri M, Bleuler H, von Moos D. High density fiber postitioner system for massive spectroscopic surveys, Monthly Notices of the Royal Astronomical Society; 2018; 481 (3); 3070-3082.

[26] Ibaraki S, Sato G, Takeuchi K. Open-loop tracking interferometer for machine tool volumetric error measurement – Two-dimensional case, Precision Engineering; 2014; 38 (3); 666-672.

[27] Ibaraki S, Nagae K, Sato G. Proposal of 'open-loop' tracking interferometer for machine tool volumetric error measurement, CIRP Annals – Manufacturing Technology; 2014; 63 (1); 501-503.

[28] Ibaraki S, Tsuboi K. Ὀpen-Loop ’Tracking Interferometer Measurement Using Rotary Axes of a Five-Axis Machine Tool, IEEE/ASME Trans. on Mechatronics; 2017; 22(5); 2342-2350.

[29] Ibaraki S, Hiruya M, A novel scheme to measure 2D error motions of linear axes by regulating the direction of a laser interferometer, Precision Engineering; 2021; 67; 152-159.

[30] Schwenke H, Franke M, Hannaford J, Kunzmann H. Error Mapping of CMMs and Machine Tools by a Single Tracking Interferometer, CIRP Annals – Manufacturing Technology; 2005.; 54(1); 475-478.

[31] Ibaraki S, Kudo T, Yano T, Takatsuji T, Osawa S, Sato O. Estimation of Three-Dimensional Volumetric Errors of Machining Centers by a Tracking Interferometer, Precision Engineering; 2013; 39; 179-186.

[32] ISO/TR 16907:2015, Numerical compensation of geometric errors of machine tools.

[33] Schwenke H, Knapp W, Haitjema H, Weckenmann A, Schmitt R, Delbressine F. Geometric Error Measurement and Compensation of Machines – An Update, CIRP Annals – Manufacturing Technology; 2008; 57(2); 560-575.

[34] Ibaraki S, Knapp W. Indirect Measurement of Volumetric Accuracy for Three-Axis and Five-Axis Machine Tools: A Review, Int. J. Automation Technology; 2012; 6 (2); 110-124.

[35] Takatsuji T, Goto M, Osawa S, Yin R, Kurosawa T. Whole-viewing-angle cat's-eye retroreflector as a target of laser trackers, Measurement Science and Technology; 1999; 10 (7); 87-90.

[36] ISO/TR 230-11:2018, Test code for machine tools – Part 11: Measuring instruments suitable for machine tool geometry tests.

[37] Li R, Zhao Y, Dynamic error compensation for industrial robot based on thermal effect model, Measurement; 2016; 88; 113-120.

[38] JCGM 101:2008, Evaluation of measurement data – Supplement 1 to the "Guide to the expression of uncertainty in measurement" – Propagation of distributions using a Monte Carlo method

[39] Bringmann B, Besuchet J, Rohr L. Systematic Evaluation of Calibration Methods, CIRP Annals – Manufacturing Technology; 2008; 57(1); 529-532.

[40] Olarra A, Axinte D, Kortaberria G. Geometrical calibration and uncertainty estimation methodology for a novel self-propelled miniature robotic machine tool, Robotics and Computer-Integrated Manufacturing; 2018; 49; 204-214.

[41] Fukuda K, Ibaraki S, Alam MM, Morita S, Usuki H, Ohtsuki N, Yoshioka H, Identification of a novel kinematic model of a 6-DOF robot with bidirectional angular positioning deviation of rotary axes, Proc. of 18th International Conference on Precision Enginee]ring (ICPE20); 2020; C-3-6.